Optimization of holographic data storage system based on Seidel aberrations reduction

Ren-Chung Liu*[a], Shiuan-Huei Lin[b], Ken-Yuh Hsu[a]

[a]Department of Photonics, National Chiao-Tung University, 1001 University Road, Hsinchu, Taiwan 300; [b] Department of Electro-physics, National Chiao-Tung University, 1001 University Road, Hsinchu, Taiwan 300

ABSTRACT

In this research, we investigate the influence of Seidel aberrations on the point spread function and the probability density function of holographic data storage systems, and thus the storage capacity and bit error rate of storage system can be obtained. The aberrations tolerances of storage systems with different numerical aperture are obtained. Optimization on BER and SC of holographic data storage systems by reducing Seidel aberrations will be demonstrated numerically.

Keywords: hologram, Seidel aberration, data storage

1. INTRODUCTION

Volume holographic data storage is regarded as a potential technology for next generation optical storage in the era of cloud computing. It has attracted intense research effort from both academia and industries [1]. Storage capacity (SC) and bit-error-rate (BER) are two parameters that are often used to evaluate the performance of holographic data storage systems. Bit errors can be induced by many factors such as material scattering, device imperfections, system misalignment, intra-page cross-talk between pixels of the same page, inter-page cross-talk between different pages, and optical aberrations, etc. When bit error occurs, it will require more error correction codes and thus the storage capacity will be degraded.

In this talk, we consider the influence of optical aberrations on BER and SC of holographic data storage systems. We describe the influence of aberrations on the point spread function and the probability density function (PDF), and thus the SC and BER can be developed. Finally, computer simulation will be presented.

2. SEIDEL ABERRATION AND MODEL ANALYSIS OF ABERRATIVE HDSS

2.1 Seidel aberration

The most popular model to describe the aberration was proposed by W. Hamilton. The aberrations are composed by Seidel aberrations and higher order aberrations. In general, the image quality is most affected by Seidel aberrations. Hence, we investigate the influence of Seidel aberrations on volume holographic storage. The generalized imaging system is shown as Fig.1.
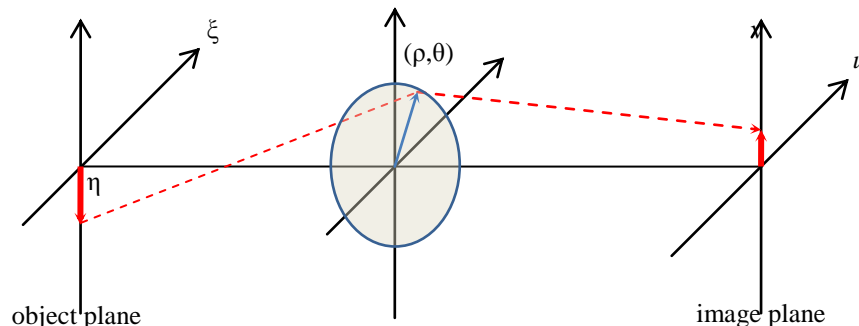

Figure 1.

*s.greg.jones@narelab.com; phone 1 222 555-1234; fax 1 222 555-876; narelab.com

where η is the height of the object, (ρ,θ) is the position of the pupil in polar-coordinate. The Seidel aberrations can be classified to five types, called spherical, coma, astigmatism, field curvature, and distortion aberrations. These aberrations can be represented in Seidel polynomials:

$$W(\eta, \rho, \theta) = \sum {}_i W_{jk} \eta^i \rho^j \cos^k \theta \ldots\ldots\ldots\ldots..\ldots\ldots\ldots\ldots\ldots.(1)$$

where ${}_iW_{jk}$ is the wavefront aberration coefficient represented by wavelengths. It means the phase errors of wavefront when the light passes the interface of lens. These five kinds of Seidel aberration are listed in Tab.1 in polar and Cartesian coordinate.

aberration type	polar coodinate	Cartesian coordinate
spherical	${}_0W_{40}\rho^4$	${}_0W_{40}\left(x^2 + y^2\right)^4$
coma	${}_1W_{31}\eta^1\rho^3\cos^1\theta$	${}_1W_{31}\eta\left(x^2 + y^2\right)y$
astigmatism	${}_2W_{22}\eta^2\rho^2\cos^2\theta$	${}_2W_{22}\eta^2 y^2$
field curvature	${}_2W_{20}\eta^2\rho^2$	${}_2W_{20}\eta^2\left(x^2 + y^2\right)$
distortion	${}_3W_{11}\eta^3\rho^1\cos^1\theta$	${}_3W_{11}\eta^3 y$

Tab.1 Seidel polynomials represented in polar and Cartesian coordinates.

2.2 Equivalent model of aberrative HDSS for point-spread-function

All the imaging system with complex optical elements can be simplified to be an equivalent model composed with input(object) plane, entrance pupil, optical system, exit pupil, and output(image) plane, consequently. The equivalent model is shown as Fig.2
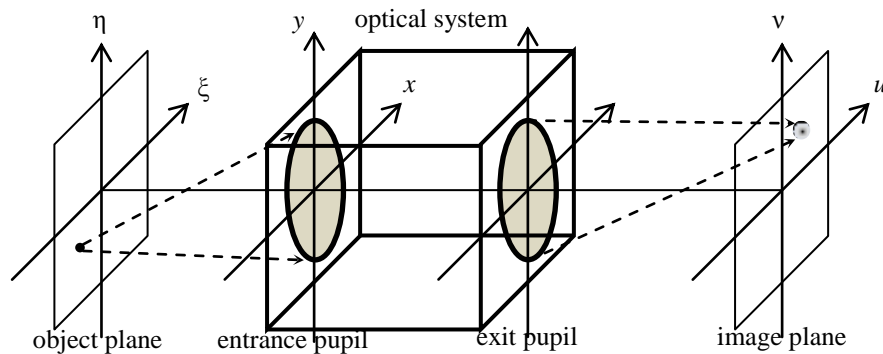

Fig.2 Equivalent model of aberrative HDSS for point-spread-function

For a linear system, the relationship between the input amplitude $O(\xi,\eta)$ and output amplitude $I(u,v)$ in coherent light case can be written as eq.(2)：

$$I(u,v) = \int\int_{-\infty}^{\infty} O(\xi,\eta) \cdot h_c(u,v;\xi,\eta)d\eta d\xi \tag{2}$$

where $h(u,v;\xi,\eta)$ is the impulse response(point spread function,PSF) of the system. For an imaging system, the impulse response is the Fourier transform of the exit pupil $P(x,y)$：

$$h_c(\xi,\eta) = \int\int_{-\infty}^{\infty} P(x,y) \cdot \exp[-i2\pi(\xi x + \eta y)]dxdy \tag{3}$$

In an aberrative imaging system, the pupil function $P'(x,y)$ is modified to be the original pupil function $P(x,y)$ multiplied with the aberration term $exp[j2\pi W(x,y)/\lambda]$ [2]：

$$P'(x,y) = P(x,y) \cdot \exp\left[j\frac{2\pi}{\lambda}W(x,y) \right] \tag{4}$$

where $W(x,y)$ is the effective length error induced by aberrations. Generally there are several lenses in a HDSS. The total aberrations can be regarded as the summation of the Seidel aberrations coefficient of each interface. Fig.3 shows that multiple surfaces of HDSS can be simplified to the generalized model.
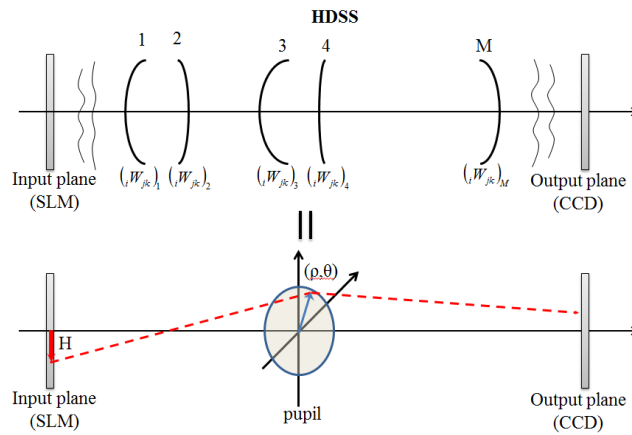

Fig.3 The generalized model of HDSS with multiple elements

The total aberration coefficient is the summation of the aberration coefficient of each surface, show as eq.(5).

$$W(H,\rho,\theta) = \sum_i W_{jk} H^i \rho^j \cos^k \theta \quad , \quad \text{where} \quad _i W_{jk} = \sum_{m=1}^{M} \left(_i W_{jk} \right)_m \tag{5}$$

2.3 Probability density function, bit-error-rate, and storage capacity

The intensity of input data bit in a holographic storage system is binary in "0"(dark state) or "1"(bright state). These data can be distorted by system noises during hologram recording and reconstruction steps. As a result, the intensity distribution of the output data will be changed to a gray level function. This distribution function can be described by a probability density function $P(I)$, where I represents the light intensity of the data bit. Fig.4 shows the schematic diagram of the volume holographic data storage system together with typical PDF distributions of input and output data.
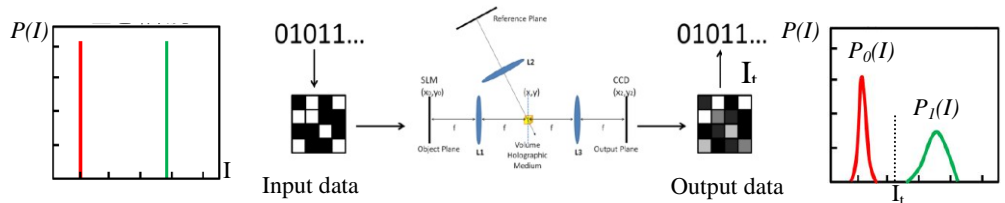

Fig.4 Volume holographic data storage system and the PDF distributions of input and

It is obvious that when the distributions of output data bit"0" and bit"1" overlap, the error bits will occur. The BER is defined as [3]:

$$BER = \pi_0 \sum_{I=I_t}^{255} P_0(I) + \pi_1 \sum_{I=0}^{I_t} P_1(I) \tag{6}$$

where π_0 and π_1 are the ratios of the numbers of bit"0" and bit"1", and $P_0(I)$ and $P_1(I)$ are PDF for the data, respectively. In analogue to communication theory a storage capacity (SC) per bit is defined as [3]:

$$SC = \sum_{I=0}^{255} \left[\pi_1 P_1(I) \cdot \log_2 \frac{P_1(I)}{\pi_1 P_1(I) + \pi_0 P_0(I)} + \pi_0 P_0(I) \cdot \log_2 \frac{P_0(I)}{\pi_1 P_1(I) + \pi_0 P_0(I)} \right] \tag{7}$$

From Eq. (6) and Eq. (7) we see that if the probability density functions of the output data are obtained, then BER and SC of the system can be calculated. The probability density function can be obtained from the point spread function of the holographic system by taking into account of the influence of Seidel aberrations.

3. SIMULATION

3.1 Aberration tolerance of HDSS with different NA

Next we will simulate the aberration tolerance of HDSS with different numerical aperture(NA). The flow chart of simulation is shown in fig.5. In the beginning, ten data pages randomly distributed with black and white pixels are generated. The resolution of each page is 1000x1000pixels. Then set the initial NA of HDSS to be 0.1. Then set aberration coefficients with incremental quantity 0.1 wavelength. After NA, aberration coefficient are set, PSF of HDSS can be obtained from eq.(4). Output data pages can be calculated from eq.(2). Then PDF of output data can be calculated. According to eq.(6) and eq.(7), BER and SC can be get. If BER is zero, increase aberration coefficient by 0.1 and run the loop again until BER is no longer zero. The aberration tolerance of HDSS with NA 0.1 is obtained. Next increase the numerical aperture, and run the loop again.
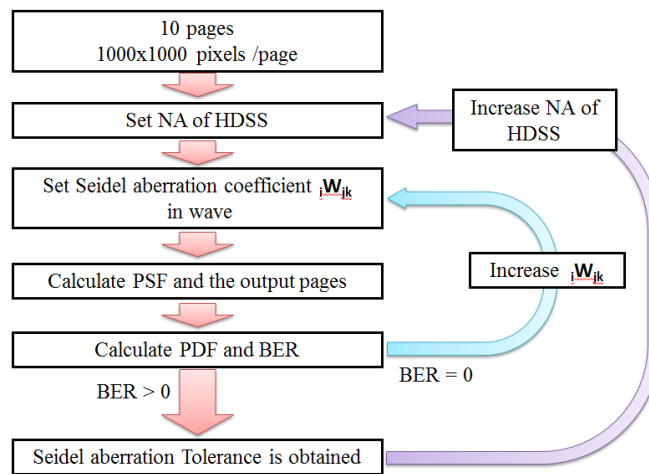
Fig.5 Flow chart for finding aberration tolerances of HDSS with different NA

Tab.2 shows simulation results of aberration tolerances of HDSS with different NA. From this table, we can know that for low NA HDSS, generally BER is dominated by the spherical aberration. For high NA HDSS, BER is dominated by distortion, field curvature, and astigmatism, respectively.

Tab.2 Aberration tolerances of HDSS with different NA

NA	0.1	0.2	0.3	0.4	0.5	0.6	0.7
Spherical $_0W_{40}$	0.3	3.4	16	50	120	260	300
Coma $_1W_{31}$	0.4	3.1	9.5	26	44	70	110
Astigmatism $_2W_{22}$	0.2	0.7	1.5	2.6	4	5.6	7.7
Field Curv. $_2W_{20}$	0.12	0.36	0.78	1.31	2.1	2.9	3.9
Distortion $_3W_{11}$	0.3	0.6	0.9	1.2	1.5	1.8	2.1

3.2 Optimal CCD pixel size of HDSS

The information capacity of each page (bits/page) is dependent on the resolution of SLM and CCD. However, the minimum bit size is limited by the PSF of HDSS. Next we simulate the PSF of a HDSS with 0.07NA. The pixel pitch of

SLM and CCD are 8.1 and 6.7 um, respectively. Two identical lens with focal length 150mm and BK7 material are used to achieve pixel match. The system arrangement is plotted in fig.6.
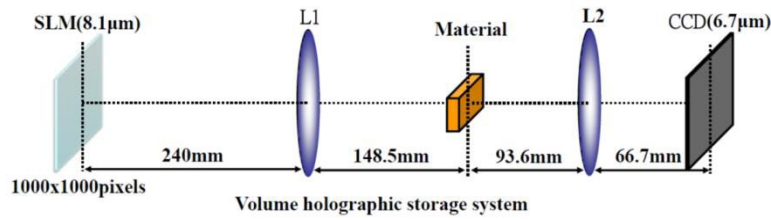

Fig.6 The system arrangement of HDSS1 with NA0.07

The wavelength is set to be 532nm. The software Zemax was used to obtain the aberration coefficients. Tab.3 shows the aberration coefficients of Seidel aberration of the HDSS1 and aberration tolerance with 0.07 NA.

Tab.3 the aberration coefficients of the HDSS1 and aberration tolerance W_{max} with 0.07 NA

Aberration coefficient	$_iW_{jk}$	W_{max}
Spherical $_0W_{40}$	8.9	0.3
Coma $_1W_{31}$	-2.6	0.4
Astigmatism $_2W_{22}$	1.2	0.2
Field Curvature $_2W_{20}$	0.5	0.12
Distortion $_3W_{11}$	-0.6	0.3

The PSF of HDSS1 can be obtained from eq.(1) and eq.(4). Then ten input data pages $O(\xi,\eta)$ are generated randomly distributed with black and white pixels. The resolution of each page is 1000x1000 pixels. The output data pages $I(u,v)$ captured on CCD can be obtained by using eq.(2). In order to optimize the bit size, 3x3, 4x4, 5x5, and 6x6 pixels are used to present 1 bit respectively. Then PDF was calculated from the output data pages by counting the bit numbers versus intensity level. Tab.4 shows the PDF, bits/pa ge, BER, and SC of HDSS1 with different bit sizes.

Tab.4 PDF, bits/pa ge, BER, and SC of HDSS1 with different bit sizes.

	3x3	4x4	5x5	6x6
CCD pixels/bit				
PDF				
BER	0.14	0.01	7.5×10^{-5}	0
Bits/page	110 kb	62.5 kb	40 kb	27.6 kb

The results shows that one bit represented by 5x5 pixels is good enough to achieve low BER ($<10^{-3}$, upper bond of BER for error bit correction) and high capacity. Fig.7 is the PSF of HDSS1 in the position (3.35, 3.35)mm of output plane on

CCD. The full width of PSF is around 30 μm. It is a good criterion to choose the CCD pixel size similar to the full width of PSF of HDSS.
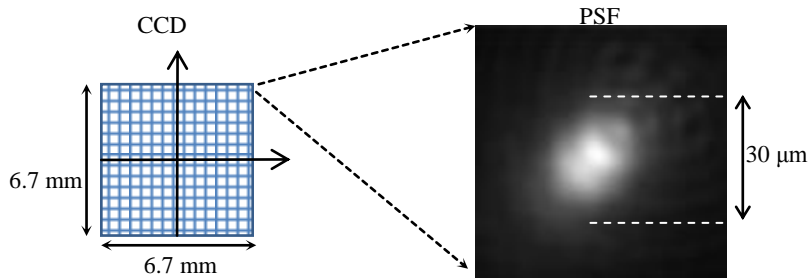

Fig.7 The PSF of HDSS1 in the position (3.35, 3.35)mm of output plane on CCD.

From Tab.3, we found that spherical aberration is the most serious one compared to the aberration tolerances. Next, an improved system HDSS2 is proposed by reducing the spherical aberration. Fig.8 shows the system arrangement of HDSS2 and corresponding aberration coefficients. The lens models of HDSS2 are Y45-171, Y45-165, Y32-996, and Y45-165, respectively from Edmund Company. The spherical aberration is reduced from 8.9 to 0.34 by changing the imaging system.

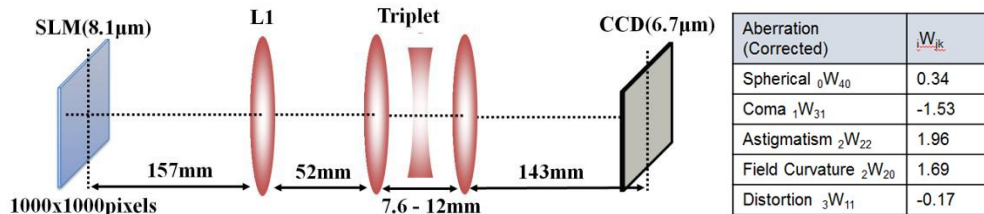| Aberration (Corrected)	$_iW_{jk}$
Spherical $_0W_{40}$	0.34
Coma $_1W_{31}$	-1.53
Astigmatism $_2W_{22}$	1.96
Field Curvature $_2W_{20}$	1.69
Distortion $_3W_{11}$	-0.17

Fig.8 The system arrangement of HDSS2 and corresponding aberration coefficients

Tab.5 shows the PDF, bits/page, BER, and SC of HDSS1(original) and HDSS2(corrected) with different bit/pixel sizes.

Tab.5 PDF, bits/page, BER, and SC of HDSS1 and HDSS2 with different bit/pixel sizes.

	PSF	4x4 pixels/bit (62.5 kbits/page)		5x5 pixels/bit (40 kbits/page)		6x6 pixels/bit (27.6 kbits/page)	
		PDF	BER	PDF	BER	PDF	BER
original			0.01		7.5×10^{-5}		0
corrected			6×10^{-4}		0		0

3.3 HDSS Performance improvement by using circular SLM

Because of the circular symmetry of Seidel aberration, the PSFs in output plane are also circularly symmetric. Fig.9 shows the distributions of PSFs of HDSS1 in output plane. The spacing of adjacent sub-photo is 0.84μm. It can be seem that PSFs are circularly symmetric. Hence, bit data in each page are arranged in circular shape to be displayed on circular SLM.
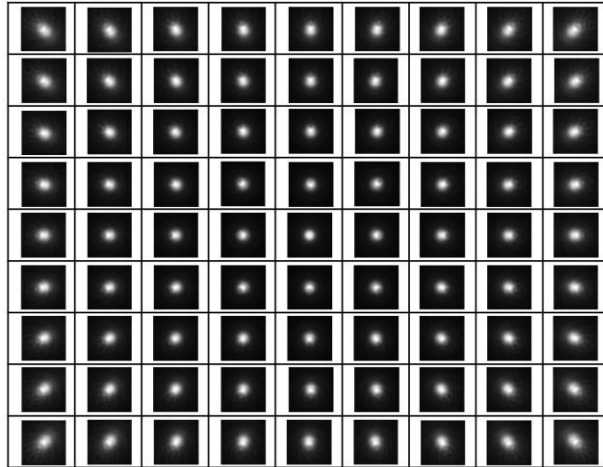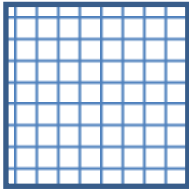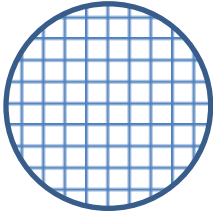
Fig.9 The distributions of PSFs of HDSS1 in output plane

Tab.6 shows the BER and SC with rectangular and circular data page. The BER of circular data pages can achieve lower BER than rectangular data pages.

Tab.6 The BER and SC with rectangular and circular data page.

SLM	rectangular	circular
BER	7.5×10^{-5}	1.4×10^{-5}
SC	0.99	0.99

4. CONCLUSION

A method for evaluating the influence of Seidel aberrations on BER and SC of HDSS is proposed. The aberration tolerances of HDSS with different NA are figured out by taking into account different kinds of Seidel aberrations. For low NA HDSS without aberration correction, spherical aberration is the most serious aberration beyond the tolerance. An improvement design by reducing spherical aberration coefficient from 8.9 to 0.3 wavelengths has been demonstrated for achieving lower BER and higher SC. Due to the circular symmetry of PSF of HDSS, the performance of HDSS can be further improved by using circular SLM to display the data pages.

REFERENCES

[1] Hans J. Coufal, Demetri Psaltis, Glenn T. Sincerbox, *Holographic Data Storage*, Springer, New York, 2000.

[2] Joseph W. Goodman, "Introduction to Fourier Optics", third edition, Englewood Colorado, ROBERTS & COMPANY, p.145-147, 2005.

[3] Neifeld, M. A. and W. C. Chou. "Information theoretic limits to the capacity of volume holographic optical memory." *Applied Optics* 36(2): Optical Society of America, 514-517, 1997.

ACKNOWLEDGEMENT